

Trajectory-free ionization times in strong-field ionization

Nicolas Eicke* and Manfred Lein

Institut für Theoretische Physik, Leibniz Universität Hannover, Appelstraße 2, 30167 Hannover, Germany

(Received 18 August 2017; published 9 March 2018)

Using a purely quantum mechanical approach without trajectories, we are able to compute momentum-resolved ionization times of electrons released by the strong-field ionization of atoms. For the attoclock setting, we show that the dominant emission angle corresponds well to instantaneous ionization at the maximum field if geometrical factors are taken into account appropriately and if the field intensity is small enough to avoid depletion of the bound state.

DOI: [10.1103/PhysRevA.97.031402](https://doi.org/10.1103/PhysRevA.97.031402)

A central achievement of strong-field physics is the ability to resolve ultrafast physical processes in atoms and molecules on the attosecond time scale. In particular, several methods have been developed to measure ionization times, i.e., to answer the question at precisely what time an electron is released from an atom in single-photon or strong-field ionization. Shafir *et al.* have used an orthogonal two-color field in high-harmonic generation as a gate to measure ionization time as a function of harmonic order [1]. Schultze *et al.* have measured a time delay of electron emission from the neon $2p$ subshell relative to the neon $2s$ subshell using extreme-ultraviolet-induced ionization in combination with an attosecond streak camera [2]. Klünder *et al.* have measured a similar time delay in argon [3]. A conceptually elegant approach to measure ionization times is attosecond angular streaking implemented by Eckle *et al.* [4], also known as the “attoclock.” The idea behind the attoclock is that in strong-field ionization with a circularly polarized laser pulse, the time of ionization is mapped to the detection angle of the photoelectron. In fact, the strong-field approximation (SFA), in which the atomic potential is neglected, provides a mapping from the photoelectron momentum distribution (PMD) to complex ionization time in a way that the real part of a given ionization time corresponds to exactly one angle [5,6]. If one breaks the rotational symmetry of the PMD by using a short pulse (or a slightly elliptically polarized field), the maximum of the SFA signal exactly corresponds to ionization at the time of peak field strength and it is obtained in the direction perpendicular to the electric field at the ionization time, provided that the envelope is chosen symmetric and the initial state is compatible with that symmetry. The maximum is found at the same position when a short-range potential is used in a numerical solution of the time-dependent Schrödinger equation (TDSE) [7]. In reality, the long-range atomic potential plays an important role, and one finds that the PMD is rotated forward with respect to the handedness of the electric field [8,9]. This could be caused by delayed ionization but also by the influence of the atomic potential on the electron after ionization. The latter prevents reading the ionization time simply from the hand of the clock. Instead, measurements

have to be cleared of this effect to make the ionization time accessible again. Often, a semiclassical model consisting of a tunneling step and subsequent motion on a classical trajectory in the combined potential generated by the laser field and the atom is used for this purpose. In this way, Eckle *et al.* could give a small upper limit on delay times in helium in a narrow range of intensities in the near infrared [8]. Pfeiffer *et al.* included the Stark shift and used initial conditions derived from a separation of the Schrödinger equation in parabolic coordinates [tunnel ionization in parabolic coordinates with induced dipole and Stark shift (TIPIS)] to get vanishing ionization times in helium and argon within the experimental accuracy over a wide range of intensities [10]. Later, Landsman *et al.* obtained a small positive tunneling delay using the same method [11]. Camus *et al.* also measured positive time delays in rare gases [12], but using a different theoretical model that predicts nonvanishing parallel velocities at the tunnel exit. Recently, analytical R -matrix (ARM) theory was used together with pulse-envelope corrections to evaluate Coulomb corrections to ionization times in an attoclock setup [7,13]. Another theoretical method is classical backpropagation [14,15]. In both cases vanishing ionization-time delay in the hydrogen atom was concluded. In rare-gas atoms there is the question whether multielectron dynamics has an additional effect on the angular offset, but at least for the helium atom this is not the case [16,17].

All attoclock-based determinations of ionization times require a theoretical model to map a given electron momentum to its ionization time. Once such a model is available, one may check, e.g., whether the momentum at the maximum signal corresponds to ionization at the peak of the pulse. The notion of some sort of electron trajectory is common to all previously used attoclock models. By contrast, in this Rapid Communication, we present a method without trajectories to retrieve ionization times. Trajectory-free methods were also presented by Yuan *et al.* [18] and by Teeny *et al.* [19]. The former consists of observing the instantaneous overlap with the bound states of the field-free system; the latter observes the probability flow through the tunnel exit. Both give large positive ionization-time delays for their respective definitions of the maximum instantaneous ionization rate, but they do not offer a momentum-resolved retrieval, which is the content of our work.

*nicolas.eicke@itp.uni-hannover.de

Our method is based on finding stationary points of the exact (non-SFA) Dyson integral. Starting from the time-dependent Schrödinger equation in the single-active-electron approximation (atomic units are used unless stated otherwise),

$$i \frac{\partial}{\partial t} |\psi(t)\rangle = \left(\frac{1}{2} \hat{\mathbf{p}}^2 + V(\mathbf{r}) \right) |\psi(t)\rangle + H_I(t) |\psi(t)\rangle, \quad (1)$$

with the interaction Hamiltonian

$$H_I(t) = \begin{cases} \mathbf{E}(t) \cdot \mathbf{r}, & \text{length gauge,} \\ \mathbf{A}(t) \cdot \hat{\mathbf{p}} + \mathbf{A}(t)^2/2, & \text{velocity gauge,} \end{cases} \quad (2)$$

and the field $\mathbf{E}(t) = -\partial_t \mathbf{A}(t)$, the Dyson integral

$$\mathcal{M}(\mathbf{p}) = -i \int_0^T dt \mathcal{D}(\mathbf{p}, t) \quad (3)$$

gives the momentum distribution $|\mathcal{M}(\mathbf{p})|^2$ of the photoelectron after ionization. The integrand is given by

$$\mathcal{D}(\mathbf{p}, t) = \langle \psi_{\mathbf{p}}^{(-)} | U(T, t) H_I(t) U_0(t, 0) | \psi_0 \rangle, \quad (4)$$

where U_0 denotes the field-free time-evolution operator with the Hamiltonian $H_0 = \hat{\mathbf{p}}^2/2 + V$ and U the full time-evolution operator. In the SFA, the scattering state $\langle \psi_{\mathbf{p}}^{(-)} |$ is replaced by a plane wave $\langle \mathbf{p} |$ and the full time-evolution operator U is approximated by the Volkov time evolution U_V which neglects the atomic potential. This leads to the amplitude

$$\mathcal{M}_{\text{SFA}}(\mathbf{p}) = -i \int_0^T dt M(\mathbf{p}, t) e^{-iS(\mathbf{p}, t)} \quad (5)$$

with the action

$$S(\mathbf{p}, t) = -I_P t + \int_t^T dt' \frac{1}{2} [\mathbf{p} + \mathbf{A}(t')]^2 \quad (6)$$

and the transition matrix element

$$M(\mathbf{p}, t) = \begin{cases} \langle \mathbf{p} + \mathbf{A}(t) | \mathbf{E}(t) \cdot \mathbf{x} | \psi_0 \rangle, & \text{length gauge,} \\ \langle \mathbf{p} | \mathbf{A}(t) \cdot \hat{\mathbf{p}} + \mathbf{A}(t)^2/2 | \psi_0 \rangle, & \text{velocity gauge.} \end{cases} \quad (7)$$

The SFA amplitude (5) is frequently evaluated using the saddle-point approximation. There, the integral is replaced by a discrete sum over stationary points of the action (6) which are given by

$$\frac{1}{2} [\mathbf{p} + \mathbf{A}(t_s)]^2 + I_P = 0. \quad (8)$$

This associates a discrete set of complex ionization times t_s with every momentum \mathbf{p} .

In this work, we retrieve ionization times including Coulomb effects by finding the stationary points of the integrand (4) directly. To this end, we solve the saddle-point equations

$$\frac{\partial}{\partial t} \mathcal{D}(\mathbf{p}, t) |_{t=t_s} = 0. \quad (9)$$

Note that this definition gives the ionization time t_s directly and makes no assumptions or statements about the tunneling time, i.e., the time the electron spends in the classically forbidden region. Saddle-point solutions to a semiclassical approximation of the Dyson integrand (4) were also considered

by Klaiber *et al.* [20]. There, the saddle-point evaluation was extended to the position coordinate to find the initial conditions for Newtonian trajectories. This leads to saddle-point times before the peak of the field, followed by a nonzero tunneling delay. Instead, we proceed with a full numerical solution here. The time derivative on the left-hand side of (9) is evaluated using the second-order central finite-difference formula. The integrand itself, Eq. (4), is evaluated by numerical wavefunction propagation starting at some time t with an initial state

$$H_I(t) U_0(t, 0) | \psi_0 \rangle \quad (10)$$

using the full time-evolution operator first down to the real axis and then along the real axis to some final time T [21]. Therefore, for each evaluation of (9), one has to solve the TDSE twice. Fortunately, solving the TDSE gives the values of $\mathcal{D}(\mathbf{p}, t)$ for all momenta at once such that it is straightforward to find the momenta \mathbf{p} for which a given t_s is a saddle-point time.

The time propagation is performed using the split-operator method with step size $dt = 0.01$ on a two-dimensional Cartesian grid with 2048 points and a box size of 400 a.u. in each direction. We use the soft-core potential

$$V(\mathbf{r}) = \frac{-1}{\sqrt{\mathbf{r}^2 + \alpha}}, \quad (11)$$

where $\alpha = 0.64$ is chosen in order to reproduce approximately the ionization potential $I_P = 0.5$ of hydrogen. The vector potential is

$$\begin{aligned} A_x(t) &= -A_0 \cos(\omega t/4)^4 \cos(\omega t), \\ A_y(t) &= -A_0 \cos(\omega t/4)^4 \sin(\omega t), \end{aligned} \quad (12)$$

representing a two-cycle circularly polarized laser pulse with $\omega = 0.05695$ corresponding to 800-nm wavelength. The field is chosen exactly as in Ref. [7]. We solve the TDSE both on the real axis to obtain momentum distributions for various intensities and in the complex plane to find the ionization times. Time propagation is always performed in velocity gauge. To evaluate $\mathcal{D}(\mathbf{p}, t)$ in the length gauge we apply the interaction operator $H_I(t)$ in the length gauge and perform a gauge transformation to the velocity gauge at time t . Starting from this complex time t , we propagate the states first down to the real axis and then along the real axis to the final time $T = 1000$. While propagating along the real axis, outgoing parts of the wave function are projected onto Volkov states starting at a distance of 150 a.u. from the atom [22].

The momentum distribution for the field strength $E_0 = 0.05$ (1.75×10^{14} W/cm²) is shown in Fig. 1(a). The distribution is clearly rotated towards positive angles. Since the maximum of the momentum distribution is expected to be formed by ionization close to the time of peak field strength, we begin by asking what momentum corresponds to ionization at the center of the pulse. To this end, we solve the saddle-point equation (9) for the momentum \mathbf{p} at $\text{Re}(t) = 0$ and varying imaginary parts $\text{Im}(t)$. It is convenient to consider the logarithmic time

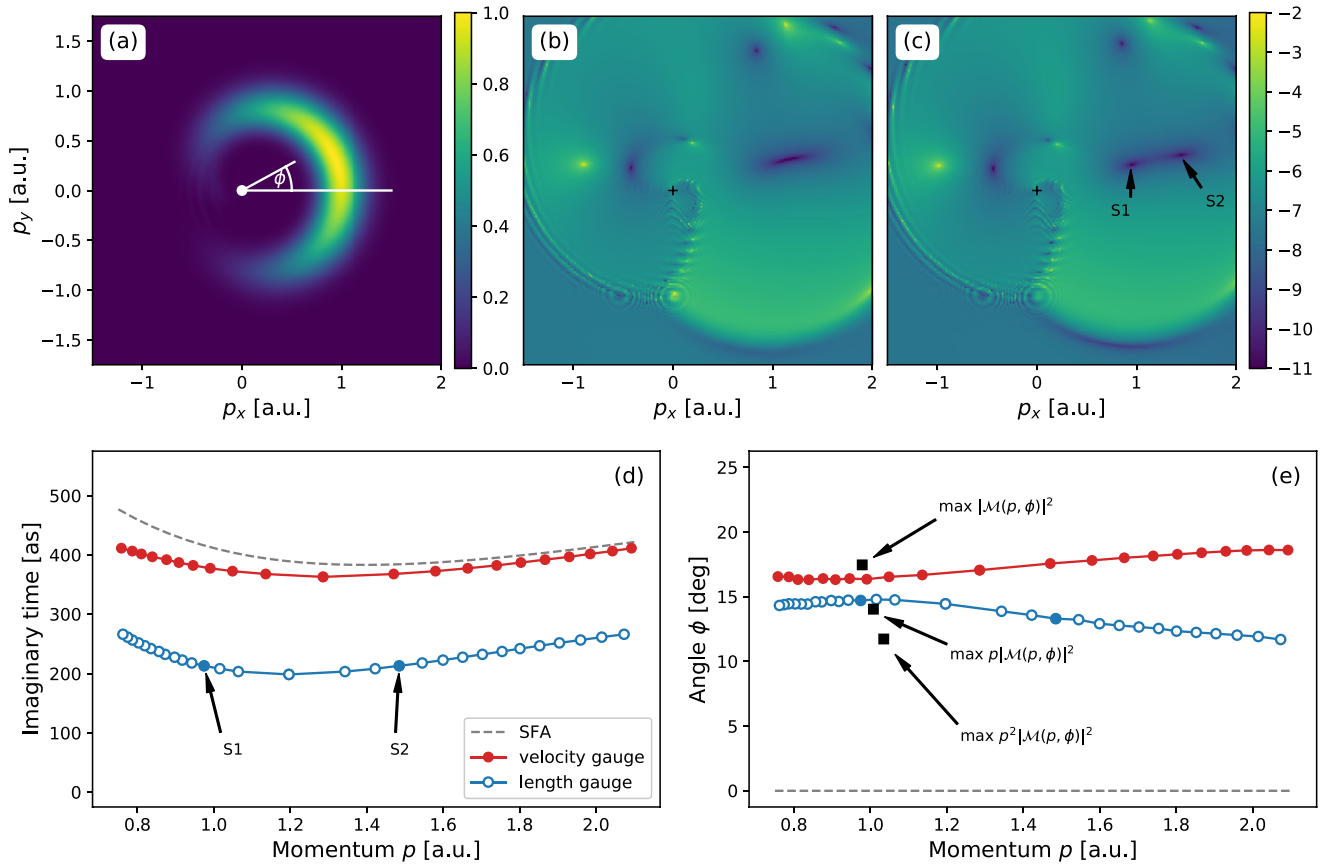


FIG. 1. (a) Photoelectron momentum distribution for $E_0 = 0.05$, normalized to maximum signal 1.0. (b), (c) Absolute value of logarithmic derivative (13) at time zero for different imaginary times (length gauge, log scale in arbitrary units). (b) $\text{Im}(t) = 198$ as. (c) $\text{Im}(t) = 213$ as. (d) Imaginary times of saddle points vs absolute value of the momentum at time zero. (e) Rotation angles of saddle points vs absolute value of the momentum at time zero. The SFA curves in (d) and (e) are obtained by solving the saddle-point equations (8) at $\text{Re}(t_s) = 0$.

derivative

$$\frac{\partial}{\partial t} \ln[\mathcal{D}(\mathbf{p}, t)] = \frac{1}{\mathcal{D}(\mathbf{p}, t)} \frac{\partial}{\partial t} \mathcal{D}(\mathbf{p}, t), \quad (13)$$

which can also be calculated for all \mathbf{p} at once.

Logarithmic derivatives for two different imaginary times are depicted in Figs. 1(b) and 1(c). For small imaginary times, no saddle points are found. For a critical value of the imaginary time, a saddle point emerges [Fig. 1(b)], which then splits into two separate saddle points for higher values of the imaginary time [Fig. 1(c)]. Comparing with Fig. 1(a), we see that the saddle points are rotated in the same direction as the momentum distribution. The exact values of these angles and the corresponding imaginary times are shown in Figs. 1(d) and 1(e) as a function of the absolute value of the momentum for both length and velocity gauge. While a photoelectron momentum distribution as an observable quantity must be independent of the choice of gauge, the same is not true for the integrand in Eq. (4). The latter is not directly observable, and so the resulting ionization times and the angles corresponding to ionization at time zero do not have to be gauge independent. Indeed, in the length gauge, saddle points emerge at much smaller imaginary times compared to the velocity gauge. The velocity-gauge saddle points are closer to the original SFA saddle points that take only the action into account. (For a strict

comparison with the SFA, one would have to find saddle points of the entire SFA integrand, not just the action.) However, the rotation angles are not so different in both gauges, especially in the region where the momentum distribution is actually concentrated. Still, for the purpose of interpreting the saddle points as ionization times, we believe that the length gauge should be favored over the velocity gauge. This is because in the length gauge, the form of the integrand (4) in the Dyson integral is closer to our interpretation of the time evolution of a bound electron until time t , followed by ionization and subsequent propagation in both the laser field and potential. The reason is that the state $U_0(t, 0)|\psi_0\rangle$ which appears in $\mathcal{D}(\mathbf{p}, t)$ in both gauges is a good approximation for the bound state in the presence of the field only in the length gauge [23].

When comparing the saddle points with the rotation angle from the momentum distribution, care must be taken in defining that angle. The most likely momentum is given by the maximum of the Cartesian distribution $|\mathcal{M}(\mathbf{p})|^2$. However, applying a semiclassical picture with an ionization and a propagation step to the present situation, the momentum that corresponds to the highest instantaneous ionization rate is the maximum of the cylindrical distribution $p|\mathcal{M}(\mathbf{p})|^2$ rather than that of the Cartesian distribution. In a recent study using ARM theory, the maximum of the spherical distribution $p^2|\mathcal{M}(\mathbf{p})|^2$ was used [7]. Many experiments, on the other hand, use the

maximum of the angular distribution to define the rotation angle [8,11,12], which in our two-dimensional (2D) case reads

$$w(\phi) = \int_0^\infty dp p |\mathcal{M}(p, \phi)|^2. \quad (14)$$

The angles we obtain from the momentum distribution according to the different criteria are shown in Fig. 1(e). We find that the angle of the Cartesian distribution is larger than the angle of the cylindrical distribution, which in turn is larger than the angle of the spherical distribution. This can be intuitively understood as a consequence of the momentum factors in the definitions of the different distributions pushing the maximum of the momentum distribution to higher momenta where the rotation angle is smaller. The angle obtained for the angular distribution (not shown here) agrees well with the cylindrical distribution. The differences between the various options are not negligible. For example, the angles from $|\mathcal{M}(\mathbf{p})|$ and $p|\mathcal{M}(\mathbf{p})|$ differ by $\Delta\phi = 3.42^\circ$, corresponding to a time difference of $\Delta\phi/\omega = 25.4$ as. In other words, the location of the maximum in a momentum distribution is influenced significantly by geometrical arguments and not only by the instantaneous ionization rate. This was also observed in Ref. [13], but its significance for the ionization-time retrieval was not addressed.

Since the angles extracted from the saddle points are almost constant as a function of radial momentum in the vicinity of the maxima, we can assign a single rotation angle to time zero, which for simplicity we take to be the one at the radial momentum given by the maximum of the cylindrical distribution. The angles obtained in this way are shown in Fig. 2(a) as a function of intensity in comparison with the angles extracted directly from the momentum distributions. For the latter, we see that the choice of prescription (Cartesian, cylindrical, spherical) has a non-negligible effect. We find good agreement between both length- and velocity-gauge saddle points and the maxima from the momentum distributions at small to intermediate field strengths. At high intensities there is disagreement. This is not surprising considering that the PMD is strongly affected by depletion whereas the ionization times are not [see Fig. 2(b)].

Finally, we proceed in analogy with previous attoclock studies [7,8] to retrieve the ionization time from the location of the peak of the PMD. Specifically, we match the saddle point in the length gauge to the maximum of the cylindrical momentum distribution. To this end, we solve Eq. (9) at a fixed value of \mathbf{p} using Newton's method. As starting values we take the imaginary parts from time zero and estimate the real parts according to $t_r = -\Delta\phi/\omega$, where $\Delta\phi$ is the difference between the time-zero angles [open circles in Fig. 2(a)] and the angles from the momentum distributions [red squares in Fig. 2(a)]. Our final result is shown in Fig. 2(c). Similar to previous studies [7,13,14], the ionization time is close to zero and never positive. Negative times that occur at higher intensities are expected because of depletion [7].

In conclusion, we have obtained momentum-resolved ionization times without resorting to electron trajectories. The theory is independent of assumptions on the initial conditions for Newtonian motion, which have often been a cause of major discussion in previous work. In the future, we plan

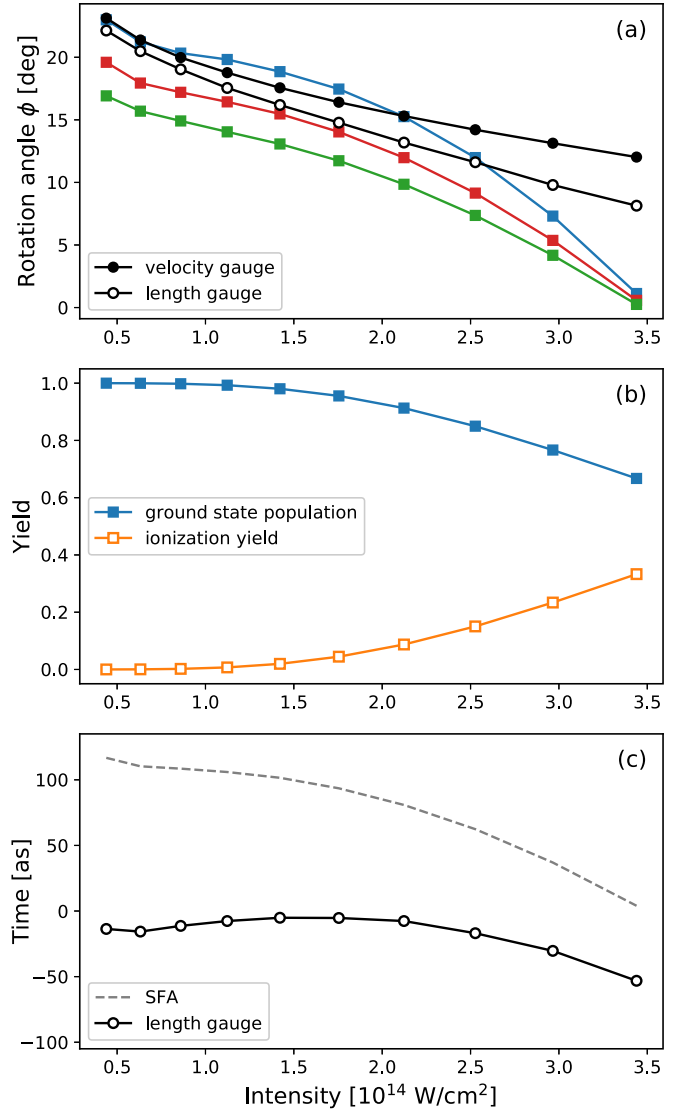


FIG. 2. (a) Rotation angles for ionization at time zero (circles) vs intensity in comparison with rotation angles from the PMDs (squares). The blue (upper) curve gives the angles at the maxima of the Cartesian PMDs, and the red (middle) and green (lower) curves show the angles from the cylindrical and spherical PMDs, respectively. (b) Ground-state population and ionization yield. (c) Retrieved ionization times corresponding to the maximum of the cylindrical distribution. The SFA curve gives the real part of the ionization time according to Eq. (8) and neglects the Coulomb correction.

to apply our method to strong-field ionization in other types of laser pulses, such as bicircular fields, and to validate our saddle-point approximation by actual evaluation of the photoelectron spectrum. Since the Dyson integral is a rather general concept in quantum mechanics, we believe that our proposal may have applications even outside strong-field ionization. It could reveal temporal aspects of bound-state dynamics or photochemistry, for example.

We acknowledge fruitful discussions with Simon Brennecke. This work has been supported by the Deutsche Forschungsgemeinschaft through the Priority Programme *Quantum Dynamics in Tailored Intense Fields* (QUTIF).

- [1] D. Shafir, H. Soifer, B. D. Bruner, M. Dagan, Y. Mairesse, S. Patchkovskii, M. Ivanov, O. Smirnova, and N. Dudovich, Resolving the time when an electron exits a tunnelling barrier, *Nature (London)* **485**, 343 (2012).
- [2] M. Schultze, M. Fieß, N. Karpowicz, J. Gagnon, M. Korbman, M. Hofstetter, S. Neppl, A. L. Cavalieri, Y. Komninos, T. Mercouris, C. A. Nicolaides, R. Pazourek, S. Nagele, J. Feist, J. Burgdörfer, A. M. Azzeer, R. Ernstorfer, R. Kienberger, U. Kleineberg, E. Goulielmakis, F. Krausz, and V. S. Yakovlev, Delay in photoemission, *Science* **328**, 1658 (2010).
- [3] K. Klünder, J. M. Dahlström, M. Gisselbrecht, T. Fordell, M. Swoboda, D. Guénot, P. Johnsson, J. Caillat, J. Mauritsson, A. Maquet, R. Taïeb, and A. L’Huillier, Probing Single-Photon Ionization on the Attosecond Time Scale, *Phys. Rev. Lett.* **106**, 143002 (2011).
- [4] P. Eckle, M. Smolarski, P. Schlup, J. Biegert, A. Staudte, M. Schöffler, H.G. Müller, R. Dörner, and U. Keller, Attosecond angular streaking, *Nat. Phys.* **4**, 565 (2008).
- [5] P. Salières, B. Carré, L. Le Déroff, F. Grasbon, G. G. Paulus, H. Walther, R. Kopold, W. Becker, D. B. Milošević, A. Sanpera, and M. Lewenstein, Feynman’s path-integral approach for intense-laser-atom interactions, *Science* **292**, 902 (2001).
- [6] D. B. Milošević, G. G. Paulus, D. Bauer, and W. Becker, Above-threshold ionization by few-cycle pulses, *J. Phys. B* **39**, R203 (2006).
- [7] L. Torlina, F. Morales, J. Kaushal, I. Ivanov, A. Kheifets, A. Zielinski, A. Scrinzi, H. G. Müller, S. Sukiasyan, M. Ivanov, and O. Smirnova, Interpreting attoclock measurements of tunnelling times, *Nat. Phys.* **11**, 503 (2015).
- [8] P. Eckle, A. N. Pfeiffer, C. Cirelli, A. Staudte, R. Dörner, H. G. Müller, M. Büttiker, and U. Keller, Attosecond ionization and tunneling delay time measurements in helium, *Science* **322**, 1525 (2008).
- [9] C. P. J. Martiny, M. Abu-samha, and L. B. Madsen, Counterintuitive angular shifts in the photoelectron momentum distribution for atoms in strong few-cycle circularly polarized laser pulses, *J. Phys. B* **42**, 161001 (2009).
- [10] A. N. Pfeiffer, C. Cirelli, M. Smolarski, D. Dimitrovski, M. Abu-samha, L. B. Madsen, and U. Keller, Attoclock reveals natural coordinates of the laser-induced tunnelling current flow in atoms, *Nat. Phys.* **8**, 76 (2012).
- [11] A. S. Landsman, M. Weger, J. Maurer, R. Boge, A. Ludwig, S. Heuser, C. Cirelli, L. Gallmann, and U. Keller, Ultrafast resolution of tunneling delay time, *Optica* **1**, 343 (2014).
- [12] N. Camus, E. Yakaboylu, L. Fechner, M. Klaiber, M. Laux, Y. Mi, K. Z. Hatsagortsyan, T. Pfeifer, C. H. Keitel, and R. Moshhammer, Experimental Evidence for Quantum Tunneling Time, *Phys. Rev. Lett.* **119**, 023201 (2017).
- [13] J. Kaushal, F. Morales, L. Torlina, M. Ivanov, and O. Smirnova, Spin-orbit Larmor clock for ionization times in one-photon and strong-field regimes, *J. Phys. B* **48**, 234002 (2015).
- [14] H. Ni, U. Saalmann, and J. M. Rost, Tunneling Ionization Time Resolved by Backpropagation, *Phys. Rev. Lett.* **117**, 023002 (2016).
- [15] H. Ni, U. Saalmann, and J. M. Rost, Tunneling exit characteristics from classical backpropagation of an ionized electron wave packet, *Phys. Rev. A* **97**, 013426 (2018).
- [16] C. Hofmann, A. S. Landsman, A. Zielinski, C. Cirelli, T. Zimmermann, A. Scrinzi, and U. Keller, Interpreting electron-momentum distributions and nonadiabaticity in strong-field ionization, *Phys. Rev. A* **90**, 043406 (2014).
- [17] V. P. Majety and A. Scrinzi, Absence of electron correlation effects in the helium attoclock setting, *J. Mod. Opt.* **64**, 1026 (2017).
- [18] M. Yuan, P. Xin, T. Chu, and H. Liu, Exploring tunneling time by instantaneous ionization rate in strong-field ionization, *Opt. Express* **25**, 23493 (2017).
- [19] N. Teeny, E. Yakaboylu, H. Bauke, and C. H. Keitel, Ionization Time and Exit Momentum in Strong-Field Tunnel Ionization, *Phys. Rev. Lett.* **116**, 063003 (2016).
- [20] M. Klaiber, K. Z. Hatsagortsyan, and C. H. Keitel, Tunneling Dynamics in Multiphoton Ionization and Attoclock Calibration, *Phys. Rev. Lett.* **114**, 083001 (2015).
- [21] M. Hartmann, Determination of momentum-dependent ionization times in strong-field ionization, Master’s thesis, Leibniz Universität Hannover, Hannover, Germany, 2016 (unpublished).
- [22] M. Lein, E. K. U. Gross, and V. Engel, Intense-Field Double Ionization of Helium: Identifying the Mechanism, *Phys. Rev. Lett.* **85**, 4707 (2000).
- [23] D. Bauer, D. B. Milošević, and W. Becker, Strong-field approximation for intense-laser atom processes: The choice of gauge, *Phys. Rev. A* **72**, 023415 (2005).